

Stable Orthorhombic CsPbBr_3 Light Emitters: Encapsulation-Assisted In Situ Synthesis

Jinwoo Park, Kyung Yeon Jang, Song Hee Lee, Dong-Hyeok Kim, So-Hye Cho, and Tae-Woo Lee*



Cite This: *Chem. Mater.* 2023, 35, 6266–6273



Read Online

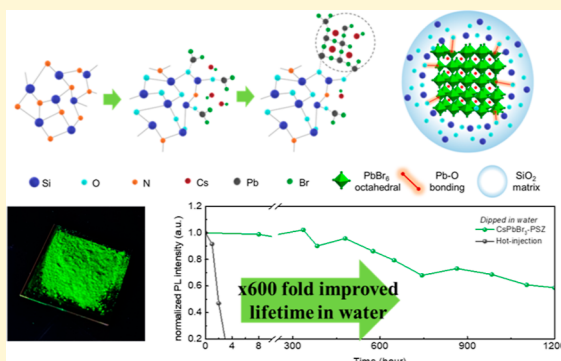
ACCESS |

Metrics & More

Article Recommendations

Supporting Information

ABSTRACT: Metal halide perovskite nanocrystals (PeNCs) are promising candidates for achieving Rec. 2020 with high color purity. However, the stability of PeNCs is inferior to that of conventional inorganic quantum dot emitters. Here, we developed a simple method using perhydropoly-silazane (PSZ) to synthesize chemically stable CsPbBr_3 PeNCs while simultaneously encapsulating them in a SiO_2 matrix. During the synthesis, PSZ converts to SiO_2 , encapsulates PeNCs, and forms stable Pb–O bonds with the orthorhombic CsPbBr_3 crystal. Unlike cubic CsPbBr_3 PeNCs synthesized by conventional colloidal synthesis, this encapsulation-assisted in situ synthesis provided orthorhombic CsPbBr_3 crystals with good control over the crystallization and with an average crystal size of 34.7 nm. Surprisingly, the resulting PeNC–PSZ composites showed a high photoluminescence quantum yield (PLQY) of 84.7% even without the use of organic ligands surrounding the PeNCs. The orthorhombic CsPbBr_3 PeNCs in situ-synthesized using PSZ assistance showed higher chemical stability than cubic CsPbBr_3 PeNCs synthesized by the conventional hot-injection method during storage under ambient conditions and in water and under continuous external energy (100 °C hot plate, UV excitation). Contrary to the common belief regarding the low stability of ionic perovskites in water, orthorhombic CsPbBr_3 PeNC in situ-synthesized using PSZ assistance retained >60% of the initial PL intensity even after long storage in water for >1100 h, which is more than 600 times longer than those of emitters that use PeNCs synthesized using the conventional hot-injection method.



1. INTRODUCTION

Metal halide perovskite nanocrystals (PeNCs) are light emitters that have greater color purity than conventional light emitters (organic, traditional inorganic quantum dots) and facile color tunability over the whole range of visible light.^{1–4} As a result, the use of PeNCs may result in the wide color gamut of the Rec. 2020 standard. Owing to their optical properties, perovskite light emitters for down-conversion applications have been rapidly developed.^{5–9} One possible strategy to obtain highly efficient PeNCs is colloidal synthesis, which exploits organic ligands.^{10–14} Organic ligands control the growth of the PeNC during colloidal synthesis and passivate the surface of the resulting PeNC. Therefore, excitons can be spatially confined in the small crystal without quenching at surface defects; thus, the photoluminescence quantum yield (PLQY) of red-, green-, and blue-emitting perovskites has been increased to near-unity.^{15,16}

However, PeNCs have low chemical stability, which is the major impediment to their commercialization for down-conversion applications. Perovskites are ionic crystals and have low formation energy, so they are vulnerable to decomposition and ion migration.^{17,18} In addition, although organic ligands surrounding PeNCs increase the PLQY, the bonds between PeNCs and organic ligands are unstable due to the dynamic nature of the ligand binding.^{19,20} Therefore, PeNCs often degrade with ligand loss during exposure to external energy (e.g.,

UV light and heat).^{21,22} Moisture induces the hydration of ligands²³ and can facilitate the aggregation and degradation of PeNCs. Aggregation shifts their PL emission wavelength (λ_{PEAK}). All these mechanisms are related to the instability of PeNCs in solid films under ambient and various harsh conditions.

The chemical stability of PeNCs can be increased by encapsulating them in an inorganic polymer such as SiO_2 or TiO_2 , which can form a steric barrier to penetration by moisture or oxygen.^{24–27} For example, PeNCs that were extremely stable in a harsh environment were synthesized using the SiO_2 matrix crosslinked from silane precursors.⁵ Chemically crosslinked matrices prevent excess water penetration and thereby reduce the hydrolysis of PeNCs and exploit the water passivation effects.⁵ Even though the inorganic encapsulation can effectively reduce or delay the reaction of moisture and perovskite crystal, only the encapsulation method cannot be the fundamental

Received: March 29, 2023

Revised: July 24, 2023

Published: August 9, 2023



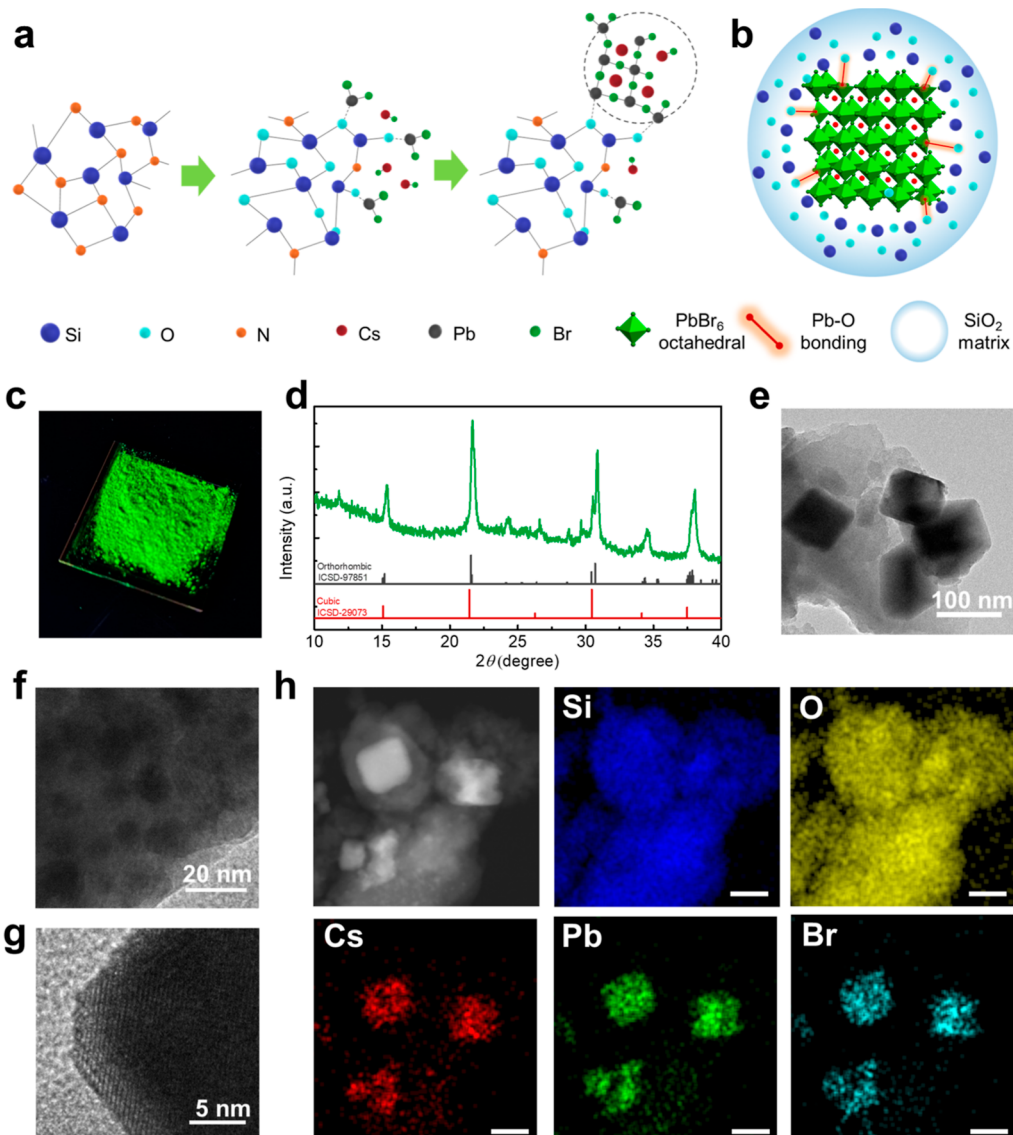


Figure 1. In situ synthesis of CsPbBr₃-PSZ composites (PSZ ratio 75 wt %). (a) Schematic illustration of the PSZ induced in situ synthesis of the CsPbBr₃ perovskite crystal and (b) resulting CsPbBr₃-PSZ composites. The red line represents covalent bonding between CsPbBr₃ and PSZ, and the blue background represents the SiO₂ matrix. (c) Photograph of CsPbBr₃-PSZ under UV light excitation. (d) XRD of CsPbBr₃-PSZ. (e,f) TEM image of CsPbBr₃-PSZ. (g) High-resolution TEM image of the CsPbBr₃ crystal. (h) EDS elemental mapping of CsPbBr₃-PSZ (scale bar: 100 nm).

solution to these effects. Penetrating chemical species can still degrade PeNCs, and acid–base reactions of PeNC ligands can inherently limit their stability.^{20,28} Therefore, a method that simultaneously controls the crystal growth of PeNCs and encapsulates them can overcome these difficulties without sacrificing the PLQY.

Here, we developed a simple one-step in situ synthesis and encapsulation method using perhydropolysilazane (PSZ) without the use of conventional small-molecule ligands such as oleic acid or oleylamine. PSZ is a SiN_x inorganic polymer that easily reacts with moisture in ambient air to form SiO₂.^{14,24,29} Simple mixing of the CsPbBr₃ precursor and PSZ followed by thermal annealing at mild temperature (100 °C) yielded CsPbBr₃-SiO₂ inorganic polymer composites (CsPbBr₃-PSZ). Crystallization of the CsPbBr₃ was controlled by the formation of a stable covalent bond between Pb in the CsPbBr₃ precursor and O in silicon oxide, so the resulting crystallized orthorhombic CsPbBr₃ was surrounded by an inorganic SiO₂ polymer. Therefore, orthorhombic CsPbBr₃ can be synthesized without the use of

organic ligands, and thus, the instability of PeNC that comes from acid–base reactions can be overcome. Unlike CsPbBr₃ synthesized by the conventional hot-injection method, synthesized CsPbBr₃ have an orthorhombic crystal structure and their in situ encapsulation enables them to achieve high PL efficiency and stability. Synthesized CsPbBr₃-PSZ composites showed a high PLQY of ~85% and highly prolonged stability under ambient conditions, under high temperature, and in water, compared with those of cubic CsPbBr₃ emitters that use PeNCs synthesized using the conventional hot-injection method.

2. EXPERIMENTAL SECTION

2.1. Materials. CsBr (99.9% trace metals basis), CsI (99.9% trace metals basis), PbBr₂ (\geq 98%), and PbI₂ (99%) were purchased from Sigma-Aldrich. Perhydropolysilazane (product number: C1SD-15001, 18.6 wt % in dibutyl ether) was obtained from Samsung SDI.

2.2. Synthesis of Perovskite-PSZ Composites. To form a perovskite precursor, 0.2 mmol of CsBr and PbBr₂ were dissolved in 1.0 mL of dimethyl sulfoxide (DMSO). This precursor was mixed with PSZ

solution dispersed in dibutyl ether at ratios of 35–85 wt % PSZ. The mixed solution of the perovskite precursor and PSZ was dropped on a substrate that had been pre-heated to 100 °C. Evaporation was performed to remove the solvent to leave a green powder in <1 min. The powder was further annealed at 100 °C for 30 min to completely remove the solvent and convert PSZ to SiO₂. To produce CsPbI₃–PSZ composites, the solution was annealed at 180 °C instead of 100 °C. Perovskite–PSZ composites were finely ground using a mortar; then, 10 mg of powder was mixed with 0.2 mL of PSZ solution and drop cast on a glass substrate to form film samples for PL measurement. The solvent was completely removed by annealing at 100 °C for 30 min.

2.3. Hot-Injection Synthesis of CsPbBr₃ Nanocrystals.

CsPbBr₃ nanocrystals were synthesized by the hot-injection method using a previously reported method with a slight modification.¹¹ Cs-oleate was prepared by dissolving 0.161 g of Cs₂CO₃ in 8 mL of pre-degassed 1-octadecene (ODE) mixed with 0.5 mL of oleic acid at 120 °C under N₂ conditions. Then, 0.069 g of PbBr₂ was dissolved in a mixture of 5 mL of ODE, 0.5 mL of oleic acid, and 0.5 mL of oleylamine, and the mixture was then degassed for 30 min. Then, 0.4 mL of Cs-oleate solution was swiftly injected at 170 °C, and the reaction was quenched in an ice bath after 5 s. The solvent was exchanged with toluene by centrifugation.

2.4. Photoluminescence and Photoluminescence Quantum Yield Measurements. Photoluminescence (PL) spectra were measured using a JASCO FP8500 spectrofluorometer. To measure the PLQYs, a 100 nm integrating sphere (ILF-835) was attached to the same spectrophotometer; PLQY values were calculated by Jasco SpectraManager II Software.

2.5. Time-Correlated Single-Photon Counting Measurements. PL lifetime and excitation-dependent measurements were measured using a FluoTime 300 fluorescence spectrometer. A picosecond-pulse laser head (LDH-P-C-405B, PicoQuant) was used to excite the samples at a wavelength of 405 nm. A photon-counting detector (PMA Hybrid 07) and a time-correlated single-photon counting (TCSPC) module (PicoHarp, PicoQuant) were used to detect the PL lifetime from samples.

2.6. Transmission Electron Microscopy Measurements.

Transmission electron microscopy (TEM) images of CsPbBr₃–PSZ composites were obtained using a JEOL-JEM 2100F microscope operating at an acceleration voltage of 200 kV.

3. RESULTS AND DISCUSSION

3.1. Synthesis and Crystal Structure of Perovskite.

Perovskite–PSZ composites were synthesized by in situ crystallization of PSZ and CsPbBr₃ (Figure 1a,b). CsPbBr₃ precursor was dissolved in DMSO, and PSZ was dissolved in dibutyl ether; then, the two solutions were mixed. The PSZ ratio in CsPbBr₃–PSZ was fixed as 75 wt %. CsPbBr₃–PSZ composites were synthesized after solvent evaporation of the mixture by annealing at a mild temperature of 100 °C. The synthesized CsPbBr₃–PSZ emitted bright-green fluorescence under UV light (Figure 1c). This in situ crystallization method using PSZ can be used to achieve different compositions by changing the precursor [CsBr to CH₃NH₃Br (MABr) to yield the MAPbBr₃ perovskite (PSZ 75 wt %); CH₂(NH₂)₂Br (FABr) to achieve the FAPbBr₃ perovskite (PSZ 60 wt %); PbBr₂ to PbI₂ to yield the CsPbBr₁I₂ perovskite (PSZ 45 wt %); and CsBr to CsI and PbBr₂ to PbI₂ to yield the CsPbI₃ perovskite (PSZ 45 wt %)], and all showed PL emission (Figure S1). However, it should be noted that we encountered difficulties in synthesizing CsPbCl₃ using our method, which could be attributed to the inherent defect intolerance of CsPbCl₃.^{30,31}

To confirm the formation of the CsPbBr₃ perovskite crystal and to check for the existence of side products, we conducted an X-ray diffraction analysis (XRD) (Figure 1d). XRD data showed only peaks that correspond well to a diffraction peak of the orthorhombic CsPbBr₃ crystal, i.e., none that corresponded to

residual CsBr or PbBr₂, or to possible side products such as Cs₄PbBr₆.^{32–34} Unlike the cubic CsPbBr₃ crystal synthesized by the conventional hot-injection method, CsPbBr₃ synthesized by PSZ assistance showed an orthorhombic crystal structure.^{11,33} Typically, the peak at $2\theta = 21.7^\circ$, which corresponds to the (200) plane of orthorhombic CsPbBr₃, showed the highest intensity and full width at half-maximum (FWHM) of $2\theta = 0.305^\circ$. From this (200) XRD peak of CsPbBr₃, the average crystal size was calculated using the Scherrer equation

$$L = \frac{K\lambda}{\beta \cos \theta}$$

where L [nm] is the average size of the crystalline domain, K is the shape factor, assumed to be 0.9, λ [nm] is the X-ray wavelength, β [rad] is the FWHM of the XRD peak, and θ [rad] is the Bragg angle. The average calculated L was 26.6 nm.

Crystallization of CsPbBr₃ perovskite crystals was further confirmed by TEM and high-resolution (HR)-TEM images (Figure 1e–g). The film consisted of crystalline regions of ~100 nm size, surrounded by amorphous regions. The crystalline regions consisted of multiple single crystals with an average size of 31.7 nm (Figures 1f and S2), which is similar to the average crystal size of 26.6 nm calculated from the XRD data. It is noteworthy that every crystal observed in HR-TEM is larger than the exciton Bohr diameter D_B (~7 nm) of CsPbBr₃. In the beyond quantum size regime where the crystal size $>D_B$, the emission wavelength and thus the FWHM of the crystal ensemble are not affected by the crystal size.^{11,35} Single crystals showed a clear 4.1 Å interplanar distance, which corresponds to the (200) plane of the orthorhombic CsPbBr₃ crystal in HR-TEM images (Figure 1g). Cs, Pb, and Br atoms were concentrated in the crystalline region, whereas Si and O atoms were evenly distributed over the whole amorphous region in energy-dispersive spectroscopy (EDS) images; this result indicates that the orthorhombic CsPbBr₃ crystal is encapsulated by the amorphous SiO₂ inorganic polymer (Figure 1h).

3.2. Chemical Binding in CsPbBr₃–PSZ Composites.

Fourier-transform infrared (FT-IR) results (Figure 2a) were obtained by reflectance mode for the pure PSZ film before annealing and for CsPbBr₃–PSZ. The results of PSZ before annealing showed sharp peaks at wavenumbers 3370 cm⁻¹ (N–H) and 2150 cm⁻¹ (Si–H), but they completely disappeared after the formation of CsPbBr₃–PSZ composites, while a broad peak at 3500–3000 cm⁻¹ (–OH) was generated. The decrease of another broad absorption at 1000–560 cm⁻¹ (related to Si–N–H and Si–N–Si bonds) and the appearance of a new sharp peak at 1040 cm⁻¹ (Si–O–Si) suggests that the silicon nitride PSZ converted to SiO₂ inorganic polymers during the formation of CsPbBr₃–PSZ composites by hydrolysis and condensation reactions.

To further analyze the chemical binding in CsPbBr₃–PSZ composites, we measured X-ray photoelectron spectroscopy (XPS) (Figures 2b and S3). XPS showed two major peaks of Pb: Pb 4f_{7/2} at 137.7 eV and Pb 4f_{5/2} at 142.6 eV, which can be deconvoluted to two peaks that differed in energy 1.1 eV, i.e., a small high-energy peak that can be attributed to Pb–O and a large low-energy peak that can be attributed to Pb–Br. This result indicates that crystallization of CsPbBr₃–PSZ composites induces binding between the CsPbBr₃ perovskite crystal and SiO₂ inorganic polymers. The direct covalent bonding between the CsPbBr₃ crystal and the stable SiO₂ matrix in CsPbBr₃–PSZ composites is distinguished from the previous study in which

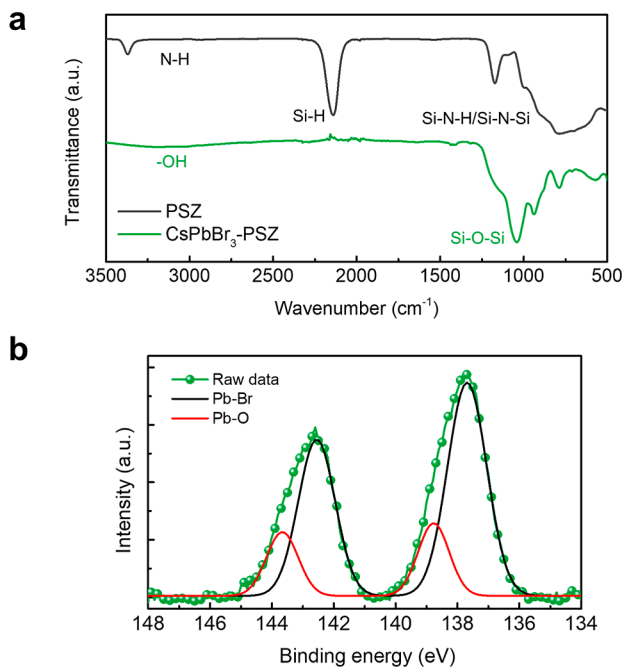


Figure 2. Chemical binding in CsPbBr₃-PSZ composites (PSZ ratio 75 wt %). (a) FT-IR data of PSZ before annealing and CsPbBr₃-PSZ composites. (b) Partial XPS result of Pb components of CsPbBr₃-PSZ.

PeNCs are bound to ligands and crosslinked with silane precursors to increase their stability.⁵

To quantify how binding between the CsPbBr₃ crystal and SiO₂ inorganic polymers affects CsPbBr₃-PSZ crystallization, CsPbBr₃-PSZ composites with PSZ ratios of 35–85 wt % were synthesized. The Pb components of the CsPbBr₃-PSZ composites with different PSZ ratios were analyzed using XPS (Figure S4a), and the resulting spectra were successfully

deconvoluted into two distinct peaks corresponding to Pb–O and Pb–Br bonding. By calculating the relative ratio of Pb–O bonding to Pb–Br based on the XPS data, we observed a gradual increase in this ratio as the PSZ ratio increased (Figure S4b). This result indicates that the increase in the ratio of PSZ in CsPbBr₃-PSZ composites increases the number of binding sites between PSZ and PbBr₂ per mole CsPbBr₃ and therefore can decrease the average crystal size. Therefore, adjusting the PSZ ratio in CsPbBr₃-PSZ composites allows for control over the crystal growth and size of perovskite while simultaneously enabling control over the average SiO₂ thickness surrounding perovskite crystals in the resulting composites.

The composite powder was further dispersed in PSZ and drop cast to fabricate thin films of the CsPbBr₃-PSZ composite. As the ratio of PSZ in the CsPbBr₃-PSZ composite was increased from 35 to 85 wt %, λ_{PEAK} gradually blue-shifted from 520 to 513 nm (Figure 3a); this result indicates increased exciton confinement as the crystal size decreased. PL lifetime trends were well correlated with steady-state PL results (Figure 3b). The abrupt PL peak wavelength shift in the 85 wt % sample is possibly related to the non-linear relationship between crystal size and the PL wavelength.^{1,35} Time-resolved PL data were fitted by the tri-exponential decay model to calculate the average lifetime (Table S1). As the PSZ ratio was increased, the average PL lifetime τ_{average} gradually decreased from 70.34 to 15.52 ns due to an increase in the strength of exciton confinement.³⁵ (Table S1). Based on the PLQY and PL lifetime, we calculated the radiative recombination rate K_r and non-radiative recombination rate K_{nr} using the following equations (Figure S5).

$$\tau_{\text{average}} = \frac{1}{K_{\text{nr}} + K_r}, \quad \text{PLQY} = \frac{K_r}{K_{\text{nr}} + K_r}$$

With increasing PSZ ratio, both K_r and K_{nr} gradually increased, indicating faster radiative recombination with stronger spatial confinement of exciton and faster non-radiative

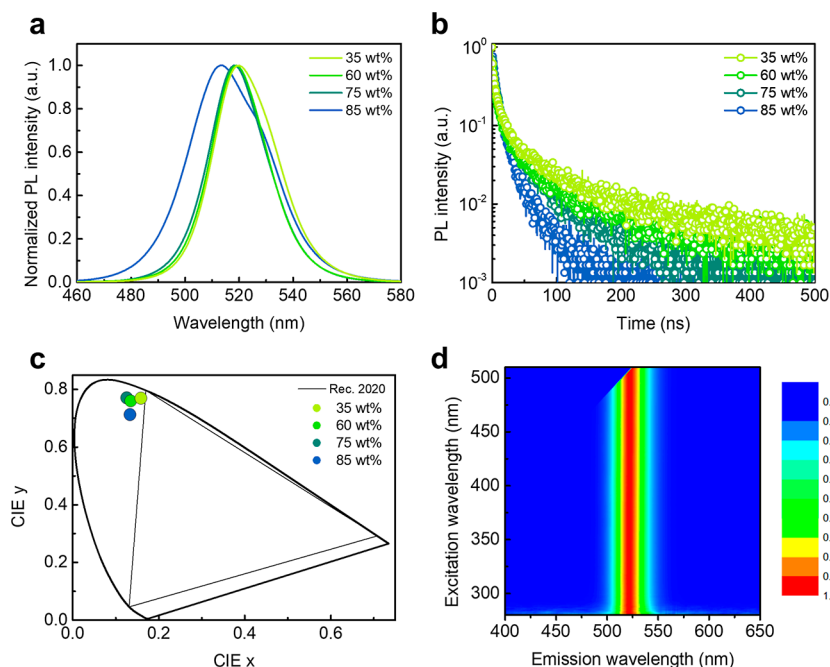


Figure 3. PL emission of CsPbBr₃-PSZ composites. (a) Steady-state, (b) time-resolved PL, and (c) CIE coordinate of CsPbBr₃-PSZ composites with different PSZ ratios ranging from 35 to 85 wt %. (d) PL emission spectra of CsPbBr₃-PSZ composites with excitation wavelengths ranging from 280 to 500 nm.

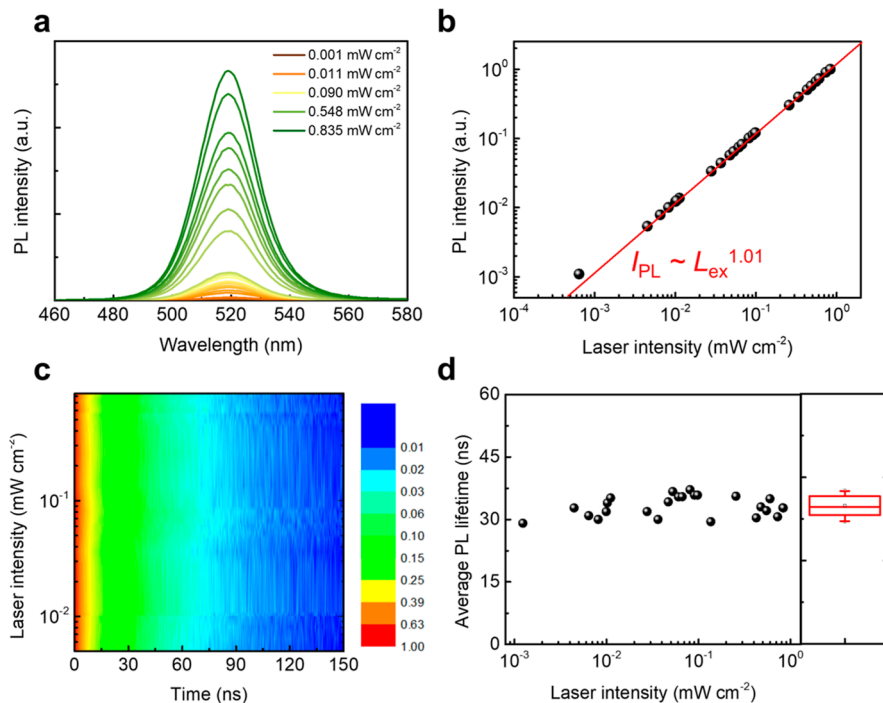


Figure 4. Excitation power-dependent PL emission of CsPbBr_3 -PSZ composites. (a) Excitation power-dependent PL spectrum and (b) integrated PL intensity of CsPbBr_3 -PSZ composites synthesized using 75 wt % PSZ. Data were fitted with $I_{PL} \sim L_{ex}^k$, whereas L_{ex} is the excitation laser intensity, I_{PL} is the integrated PL intensity, and k is the recombination factor (red line). (c) Contour plot of excitation power-dependent time-resolved PL. The color scale is set to a log scale. (d) Excitation power-dependent average PL lifetime and box plot of average PL lifetime of CsPbBr_3 -PSZ.

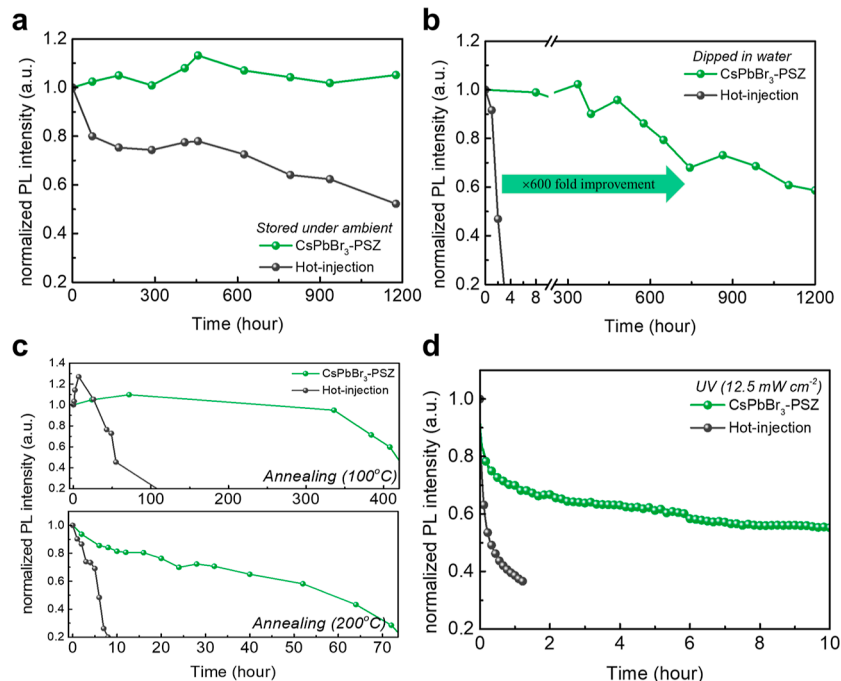


Figure 5. Stability of CsPbBr_3 -PSZ composites synthesized using PSZ assistance and using the conventional hot-injection method. Relative PL intensity change when CsPbBr_3 -PSZ composites using PSZ assistance and using the conventional hot-injection method: (a) stored under ambient conditions, (b) dipped in DI water, (c) annealed at 100 °C (top) and 200 °C (bottom), and (d) irradiated by 12.5 mW cm⁻² laser diode.

recombination resulting from a larger surface-to-volume ratio in the smaller crystal.^{35,36} Due to the trade-off effect between exciton confinement and surface-defect non-radiative recombination, CsPbBr_3 -PSZ synthesized using 75 wt % of PSZ showed the highest PLQY of 84.7%. The trend in PLQY also matches well with the binding energy of Pb–Br calculated from the XPS

results (Figure S5a). The correlation between Pb–Br binding energy and the PLQY further supports the influence of binding characteristics on the optical properties of the CsPbBr_3 -PSZ composite.

CsPbBr_3 -PSZ composites synthesized using 75 wt % of PSZ have $\lambda_{\text{PEAK}} = 518$ nm, which corresponds to the CIE coordinate

(0.128, 0.776) and a narrow FWHM of 25 nm (**Figure 3c** and **Table S2**). Combined with an ideal red emitter [CIE coordinate (0.71, 0.29)] and blue emitter [CIE coordinate (0.13, 0.05)], this CIE coordinate value could enable a wide color gamut area that can cover 133.3% of the NTSC standard and 99.6% of Rec. 2020 and a wide color gamut coverage of 92.9% of Rec. 2020 (**Table S2**). λ_{PEAK} and FWHM of CsPbBr_3 –PSZ were consistent over excitation wavelengths $280 \text{ nm} \leq \lambda_{\text{ex}} \leq 500 \text{ nm}$ (**Figure 3d**).

To analyze the recombination dynamics, we also measured the dependence of steady-state PL of CsPbBr_3 –PSZ composites on laser excitation power L_{ex} (**Figure 4a,b**). λ_{ex} was fixed at 405 nm, and the excitation laser power L_{ex} was increased from 1.24×10^{-3} to $8.35 \times 10^{-1} \text{ mW cm}^{-2}$. Integrated steady-state PL intensity I_{PL} was related to L_{ex} as $I_{\text{PL}} \sim L_{\text{ex}}^k$, where k is the recombination factor.^{37,38} The CsPbBr_3 –PSZ composites had $k = 1.01$, which indicates that the emission in the CsPbBr_3 –PSZ composites is mainly a result of excitonic recombination, in which the PL intensity is proportional to the exciton concentration.

As L_{ex} increased, I_{PL} increased linearly, but the PL lifetime remained constant with an average lifetime of 33.1 ns and a standard deviation of 2.4 ns (**Figure 4c,d**). This independence of L_{ex} and time-resolved PL results indicate that in the range of L_{ex} tested, excitonic recombination is dominant rather than bimolecular recombination of free carriers. Excitonic-dominant recombination may originate from the fine control of the crystal growth of the CsPbBr_3 perovskite by binding of CsPbBr_3 and PSZ (average crystal size <40 nm) and is well-correlated with high PLQY (~85%).

3.3. Stability of CsPbBr_3 –PSZ Composites. To compare the stability of orthorhombic CsPbBr_3 –PSZ composites, cubic CsPbBr_3 PeNCs were synthesized using the conventional hot-injection method with oleic acid and oleylamine ligands;¹¹ then, they were used to fabricate CsPbBr_3 films by identical methods to those used to fabricate films of CsPbBr_3 –PSZ composites.

Orthorhombic CsPbBr_3 –PSZ composites and the hot-injection-synthesized cubic CsPbBr_3 PeNC sample were kept under ambient conditions with an average temperature of 25 °C and a relative humidity (RH) of 60% (**Figure 5a**) or immersed in deionized water at 25 °C (**Figure 5b**), and in all cases, the time L_{60} taken for the PL intensity to decrease to 60% of the initial intensity was measured. Orthorhombic CsPbBr_3 –PSZ composites showed no noticeable degradation after >1200 h under ambient conditions, whereas the cubic PeNC sample had $L_{60} = 990$ h. Typically, orthorhombic CsPbBr_3 –PSZ composites showed remarkably improved stability against the water with $L_{60} \sim 1135$ h, which is ~600 times longer than that of cubic PeNCs synthesized by the hot-injection method, which showed rapid degradation in water with $L_{60} < 2$ h.

To test the thermal stability of the CsPbBr_3 –PSZ composites, their steady-state PL was measured while changing the temperature from 300 to 410 K and back in increments of 10 K (**Figure S6**). To stabilize the CsPbBr_3 –PSZ at each temperature and observe the effect of temperature, the composites were kept for >10 min at each temperature. The temperature did not cause a noticeable change in the λ_{PEAK} , but the PL intensity gradually decreased, and at 410 K, it was 6.4% of the original intensity at 300 K, but the loss was completely recovered after the temperature was lowered again to 300 K. The PL intensity decrease at high temperature may be a result of thermal dissociation of excitons, but temperatures ≤ 410 K did not cause irreversible degradation of CsPbBr_3 –PSZ in a short time of ~10 min.

To further test the stability of CsPbBr_3 –PSZ composites, the samples were exposed to continuous external energy of 100 and 200 °C heating (**Figure 5c**) and 12.5 mW cm^{-2} laser irradiation (**Figure 5d**). For the thermal stability measurement, we kept our sample at the set temperature on a hot plate but measured the PL intensity at room temperature to avoid thermal dissociation of the excitons. At 100 °C of heating, the orthorhombic CsPbBr_3 –PSZ sample showed a small and slow overshoot (10% of initial intensity during 72 h), retained 95% of the initial intensity during 336 h, and had L_{60} at 100 °C of >400 h. In contrast, cubic CsPbBr_3 synthesized by hot injection showed severe initial overshoot of PL intensity to 127% of the original PL intensity during 7 h of applied heating, but then the PL intensity decreased abruptly ($L_{60} \approx 50$ h). Initial overshooting of PL intensity can be attributed to the increased crystallinity of PeNC during the annealing process;³⁹ reduced PL overshooting in CsPbBr_3 –PSZ composites supported stable binding between PeNC and SiO_2 , reduced the ion migration, and increased the crystal stability against thermal energy. At an annealing temperature of 200 °C, which exceeded the preparation temperature, neither of the samples exhibited any PL overshooting, while the CsPbBr_3 –PSZ composites showed a significantly prolonged L_{60} lifetime of 48.1 h, which was 8.8 times longer compared to that of CsPbBr_3 synthesized via hot injection ($L_{60} \sim 5.44$ h).

For photo-stability measurements, we measured the PL intensity *in situ* during continuous excitation using a 405 nm laser at 12.5 mW cm^{-2} . The orthorhombic CsPbBr_3 –PSZ had a 6 times prolonged L_{60} of ~5.73 h, whereas cubic CsPbBr_3 synthesized by hot injection had $L_{60} < 1$ h.

4. CONCLUSIONS

We *in situ*-synthesized efficient and stable CsPbBr_3 perovskite crystals with assistance of PSZ by simple mixing of PSZ and the perovskite precursor. The synthesized CsPbBr_3 –PSZ composites exhibited a high PLQY of ~85%. The PL spectrum of the synthesized CsPbBr_3 –PSZ composite can be easily tuned by changing the mixing ratio of PSZ and the perovskite precursor. The synthesized CsPbBr_3 PeNCs have an orthorhombic crystal structure unlike cubic CsPbBr_3 PeNCs synthesized by the conventional hot-injection method. The orthorhombic CsPbBr_3 crystal can achieve high PLQY and stability by *in situ* formation of stable covalent bonds and encapsulation despite their different crystal structure. During the synthesis, PSZ converts to SiO_2 inorganic polymer and forms stable covalent Pb–O bonds that can overcome the dynamic nature of the ligand binding. Simultaneously, the inorganic polymer SiO_2 encapsulates the CsPbBr_3 perovskite crystal. Consequently, the synthesized CsPbBr_3 –PSZ composites showed high stability under ambient and harsh conditions. Contrary to the common belief regarding the low stability of PeNCs in water, CsPbBr_3 –PSZ showed outstanding stability in water (>60% of initial PL intensity after 1100 h). This lifetime is more than 600 times longer than those of emitters that use cubic CsPbBr_3 PeNCs synthesized using the conventional hot-injection method; *in situ* synthesis and encapsulation using PSZ have provided a route to overcome the intrinsic instability of PeNCs.

■ ASSOCIATED CONTENT

● Supporting Information

The Supporting Information is available free of charge at <https://pubs.acs.org/doi/10.1021/acs.chemmater.3c00732>.

Steady-state PL results of different compositions; crystal size distribution; XPS results and the associated analysis; PLQY and the calculated recombination rate; fitted results of time-resolved PL; emission characteristics related to the PL spectrum and color gamut; and temperature-dependent PL results ([PDF](#))

■ AUTHOR INFORMATION

Corresponding Author

Tae-Woo Lee – Department of Materials Science and Engineering, Institute of Engineering Research, Seoul National University, Seoul 08826, Republic of Korea; School of Chemical and Biological Engineering, Institute of Engineering Research, Research Institute of Advanced Materials, Soft Foundry, Seoul National University, Seoul 08826, Republic of Korea; SN Display Co. Ltd., Seoul 08826, Republic of Korea;  [0000-0002-6449-6725](https://orcid.org/0000-0002-6449-6725); Email: twlees@snu.ac.kr, taewlees@gmail.com

Authors

Jinwoo Park – Department of Materials Science and Engineering, Institute of Engineering Research, Seoul National University, Seoul 08826, Republic of Korea
Kyung Yeon Jang – Department of Materials Science and Engineering, Institute of Engineering Research, Seoul National University, Seoul 08826, Republic of Korea
Song Hee Lee – Department of Materials Science and Engineering, Institute of Engineering Research, Seoul National University, Seoul 08826, Republic of Korea
Dong-Hyeok Kim – Department of Materials Science and Engineering, Institute of Engineering Research, Seoul National University, Seoul 08826, Republic of Korea
So-Hye Cho – Materials Architecturing Research Center, Korea Institute of Science and Technology, Seoul 02792, Korea;  [0000-0001-9707-8629](https://orcid.org/0000-0001-9707-8629)

Complete contact information is available at:

<https://pubs.acs.org/10.1021/acs.chemmater.3c00732>

Author Contributions

J.P. designed the study, performed the experiments, analyzed the data, and prepared the manuscript. S.-H.L. helped to perform TEM. K.-Y.J. performed XPS, and D.H.K. performed temperature-dependent analysis. S.-H.C. contributed to data analysis. T.-W.L. designed and supervised the study, analyzed the data, and prepared the manuscript. All authors discussed the results and commented on the manuscript.

Funding

This work was supported by the National Research Foundation of Korea (NRF) grant funded by the Korean government (MSIT) (NRF-2016R1A3B1908431).

Notes

The authors declare no competing financial interest.

■ REFERENCES

- (1) Park, J.; Jang, H. M.; Kim, S.; Jo, S. H.; Lee, T.-W. Electroluminescence of Perovskite Nanocrystals with Ligand Engineering. *Trends Chem.* **2020**, *2*, 837–849.
- (2) Fakharuddin, A.; Gangishetty, M. K.; Abdi-Jalebi, M.; Chin, S.-H.; bin Mohd Yusoff, A. R.; Congreve, D. N.; Tress, W.; Deschler, F.; Vasilopoulou, M.; Bolink, H. J. Perovskite Light-Emitting Diodes. *Nat. Electron.* **2022**, *5*, 203–216.
- (3) Kim, J.-S.; Heo, J.-M.; Park, G.-S.; Woo, S.-J.; Cho, C.; Yun, H. J.; Kim, D.-H.; Park, J.; Lee, S.-C.; Park, S.-H.; Yoon, E.; Greenham, N. C.; Lee, T.-W. Ultra-Bright, Efficient and Stable Perovskite Light-Emitting Diodes. *Nature* **2022**, *611*, 688–694.
- (4) Lee, T.-W.; Im, S. H.; Cho, H.; Kim, Y.-H. Perovskite Light Emitting Device Containing Exciton Buffer Layer and Method for Manufacturing Same. U.S. Patent 10,263,207 B2, 2015.
- (5) Jang, J.; Kim, Y.-H.; Park, S.; Yoo, D.; Cho, H.; Jang, J.; Jeong, H. B.; Lee, H.; Yuk, J. M.; Park, C. B.; Jeon, D. Y.; Kim, Y.-H.; Bae, B.-S.; Lee, T.-W. Extremely Stable Luminescent Crosslinked Perovskite Nanoparticles under Harsh Environments over 1.5 Years. *Adv. Mater.* **2021**, *33*, 2005255.
- (6) Wu, X.; Ji, H.; Yan, X.; Zhong, H. Industry Outlook of Perovskite Quantum Dots for Display Applications. *Nat. Nanotechnol.* **2022**, *17*, 813–816.
- (7) Lee, H.; Park, J.; Kim, S.; Lee, S.-C.; Kim, Y.-H.; Lee, T.-W. Perovskite Emitters as a Platform Material for Down-Conversion Applications. *Adv. Mater. Technol.* **2020**, *5*, 2000091.
- (8) Lee, T.-W.; Im, S. H.; Cho, H.; Kim, Y.-H. Light-Emitting Layer for Perovskite Light-Emitting Device, Method for Manufacturing Same, and Perovskite Light-Emitting Device Using Same. U.S. Patent 10,276,807 B2, 2015. (a) Lee, T.-W.; Im, S. H.; Cho, H.; Kim, Y.-H. Perovskite light emitting element for the light emitting layer and a method of manufacturing and using the same Perovskite light emitting element. KR 101724210 B1, 2015.
- (9) Lee, T.-W.; Im, S. H.; Kim, Y.-H.; Cho, H. Perovskite Nanocrystalline Particles and Optoelectronic Device Using Same. U.S. Patent 10,193,088 B2, 2015. (a) Lee, T.-W.; Im, S. H.; Kim, Y.-H.; Cho, H. Perovskite light emitting device including exciton buffer layer and manufacturing method thereof. KR 101703451 B1, 2015.
- (10) Kim, Y.-H.; Park, J.; Kim, S.; Kim, J. S.; Xu, H.; Jeong, S.-H.; Hu, B.; Lee, T.-W. Exploiting the Full Advantages of Colloidal Perovskite Nanocrystals for Large-Area Efficient Light-Emitting Diodes. *Nat. Nanotechnol.* **2022**, *17*, 590–597.
- (11) Protesescu, L.; Yakunin, S.; Bodnarchuk, M. I.; Krieg, F.; Caputo, R.; Hendon, C. H.; Yang, R. X.; Walsh, A.; Kovalenko, M. V. Nanocrystals of Cesium Lead Halide Perovskites (CsPbX_3 , X = Cl, Br, and I): Novel Optoelectronic Materials Showing Bright Emission with Wide Color Gamut. *Nano Lett.* **2015**, *15*, 3692–3696.
- (12) Kim, Y.-H.; Kim, S.; Kakekhani, A.; Park, J.; Park, J.; Lee, Y.-H.; Xu, H.; Nagane, S.; Wexler, R. B.; Kim, D.-H.; Jo, S. H.; Martínez-Sarti, L.; Tan, P.; Sadhanala, A.; Park, G.-S.; Kim, Y.-W.; Hu, B.; Bolink, H. J.; Yoo, S.; Friend, R. H.; Rappe, A. M.; Lee, T.-W. Comprehensive Defect Suppression in Perovskite Nanocrystals for High-Efficiency Light-Emitting Diodes. *Nat. Photonics* **2021**, *15*, 148–155.
- (13) Hassan, Y.; Park, J. H.; Crawford, M. L.; Sadhanala, A.; Lee, J.; Sadighian, J. C.; Mosconi, E.; Shivanna, R.; Radicchi, E.; Jeong, M.; Yang, C.; Choi, H.; Park, S. H.; Song, M. H.; De Angelis, F.; Wong, C. Y.; Friend, R. H.; Lee, B. R.; Snaith, H. J. Ligand-Engineered Bandgap Stability in Mixed-Halide Perovskite LEDs. *Nature* **2021**, *591*, 72–77.
- (14) Han, T.-H.; Jang, K. Y.; Dong, Y.; Friend, R. H.; Sargent, E. H.; Lee, T.-W. A Roadmap for the Commercialization of Perovskite Light Emitters. *Nat. Rev. Mater.* **2022**, *7*, 757–777.
- (15) Zhou, X.; Zhang, J.; Tong, X.; Sun, Y.; Zhang, H.; Min, Y.; Qian, Y. Near-Unity Quantum Yield and Superior Stable Indium-Doped $\text{CsPbBr}_{x}\text{I}_{3-x}$ Perovskite Quantum Dots for Pure Red Light-Emitting Diodes. *Adv. Opt. Mater.* **2022**, *10*, 2101517.
- (16) Mondal, N.; De, A.; Samanta, A. Achieving Near-Unity Photoluminescence Efficiency for Blue-Violet-Emitting Perovskite Nanocrystals. *ACS Energy Lett.* **2019**, *4*, 32–39.
- (17) Kamat, P. V.; Kuno, M. Halide Ion Migration in Perovskite Nanocrystals and Nanostructures. *Acc. Chem. Res.* **2021**, *54*, 520–531.
- (18) Zhang, H.; Fu, X.; Tang, Y.; Wang, H.; Zhang, C.; Yu, W. W.; Wang, X.; Zhang, Y.; Xiao, M. Phase Segregation Due to Ion Migration in All-Inorganic Mixed-Halide Perovskite Nanocrystals. *Nat. Commun.* **2019**, *10*, 1088.
- (19) Krieg, F.; Ong, Q. K.; Burian, M.; Rainò, G.; Naumenko, D.; Amenitsch, H.; Süess, A.; Grotevent, M. J.; Krumeich, F.; Bodnarchuk, M. I.; Shorubalko, I.; Stellacci, F.; Kovalenko, M. V. Stable Ultraconcentrated and Ultradilute Colloids of CsPbX_3 (X = Cl, Br)

- Nanocrystals Using Natural Lecithin as a Capping Ligand. *J. Am. Chem. Soc.* **2019**, *141*, 19839–19849.
- (20) De Roo, J.; Ibáñez, M.; Geiregat, P.; Nedelcu, G.; Walravens, W.; Maes, J.; Martins, J. C.; Van Driessche, I.; Kovalenko, M. V.; Hens, Z. Highly Dynamic Ligand Binding and Light Absorption Coefficient of Cesium Lead Bromide Perovskite Nanocrystals. *ACS Nano* **2016**, *10*, 2071–2081.
- (21) Yuan, G.; Ritchie, C.; Ritter, M.; Murphy, S.; Gómez, D. E.; Mulvaney, P. The Degradation and Blinking of Single CsPbI_3 Perovskite Quantum Dots. *J. Phys. Chem. C* **2018**, *122*, 13407–13415.
- (22) Lee, H.; Jeong, J. W.; So, M. G.; Jung, G. Y.; Lee, C.-L. Design of Chemically Stable Organic Perovskite Quantum Dots for Micro-patterned Light-Emitting Diodes through Kinetic Control of a Cross-Linkable Ligand System. *Adv. Mater.* **2021**, *33*, 2007855.
- (23) Li, Z.-J.; Hofman, E.; Li, J.; Davis, A. H.; Tung, C.-H.; Wu, L.-Z.; Zheng, W. Photoelectrochemically Active and Environmentally Stable $\text{CsPbBr}_3/\text{TiO}_2$ Core/Shell Nanocrystals. *Adv. Funct. Mater.* **2018**, *28*, 1704288.
- (24) Jing, Y.; Merkx, M. J. M.; Cai, J.; Cao, K.; Kessels, W. M. M.; Mackus, A. J. M.; Chen, R. Nanoscale Encapsulation of Perovskite Nanocrystal Luminescent Films via Plasma-Enhanced SiO_2 Atomic Layer Deposition. *ACS Appl. Mater. Interfaces* **2020**, *12*, 53519–53527.
- (25) Duan, Y.; Ezquerro, C.; Serrano, E.; Lalinde, E.; García-Martínez, J.; Berenguer, J. R.; Costa, R. D. Meeting High Stability and Efficiency in Hybrid Light-Emitting Diodes Based on $\text{SiO}_2/\text{ZrO}_2$ Coated CsPbBr_3 Perovskite Nanocrystals. *Adv. Funct. Mater.* **2020**, *30*, 2005401.
- (26) Xu, Y.-F.; Wang, X.-D.; Liao, J.-F.; Chen, B.-X.; Chen, H.-Y.; Kuang, D.-B. Amorphous- TiO_2 -Encapsulated CsPbBr_3 Nanocrystal Composite Photocatalyst with Enhanced Charge Separation and CO_2 Fixation. *Adv. Mater. Interfaces* **2018**, *5*, 1801015.
- (27) Guo, T.; Bose, R.; Zhou, X.; Gartstein, Y. N.; Yang, H.; Kwon, S.; Kim, M. J.; Lutfullin, M.; Sinatra, L.; Gereige, I.; Al-Saggaf, A.; Bakr, O. M.; Mohammed, O. F.; Malko, A. V. Delayed Photoluminescence and Modified Blinking Statistics in Alumina-Encapsulated Zero-Dimensional Inorganic Perovskite Nanocrystals. *J. Phys. Chem. Lett.* **2019**, *10*, 6780–6787.
- (28) Zaccaria, F.; Zhang, B.; Goldoni, L.; Imran, M.; Zito, J.; van Beek, B.; Lauciello, S.; De Trizio, L.; Manna, L.; Infante, I. The Reactivity of CsPbBr_3 Nanocrystals toward Acid/Base Ligands. *ACS Nano* **2022**, *16*, 1444–1455.
- (29) Günther, M.; Wang, K.; Bordia, R. K.; Motz, G. Conversion Behaviour and Resulting Mechanical Properties of Polysilazane-Based Coatings. *J. Eur. Ceram. Soc.* **2012**, *32*, 1883–1892.
- (30) Nenon, D. P.; Pressler, K.; Kang, J.; Koscher, B. A.; Olshansky, J. H.; Osowiecki, W. T.; Koc, M. A.; Wang, L.-W.; Alivisatos, A. P. Design Principles for Trap-Free CsPbX_3 Nanocrystals: Enumerating and Eliminating Surface Halide Vacancies with Softer Lewis Bases. *J. Am. Chem. Soc.* **2018**, *140*, 17760–17772.
- (31) Zheng, X.; Hou, Y.; Sun, H.-T.; Mohammed, O. F.; Sargent, E. H.; Bakr, O. M. Reducing Defects in Halide Perovskite Nanocrystals for Light-Emitting Applications. *J. Phys. Chem. Lett.* **2019**, *10*, 2629–2640.
- (32) Zhang, M.; Zheng, Z.; Fu, Q.; Chen, Z.; He, J.; Zhang, S.; Yan, L.; Hu, Y.; Luo, W. Growth and Characterization of All-Inorganic Lead Halide Perovskite Semiconductor CsPbBr_3 Single Crystals. *CrystEngComm* **2017**, *19*, 6797–6803.
- (33) Zhang, X.; Bai, X.; Wu, H.; Zhang, X.; Sun, C.; Zhang, Y.; Zhang, W.; Zheng, W.; Yu, W. W.; Rogach, A. L. Water-Assisted Size and Shape Control of CsPbBr_3 Perovskite Nanocrystals. *Angew. Chem., Int. Ed.* **2018**, *57*, 3337–3342.
- (34) Baek, K.-Y.; Lee, W.; Lee, J.; Kim, J.; Ahn, H.; Kim, J. I.; Kim, J.; Lim, H.; Shin, J.; Ko, Y.-J.; Lee, H.-D.; Friend, R. H.; Lee, T.-W.; Lee, J.; Kang, K.; Lee, T. Mechanochemistry-Driven Engineering of 0D/3D Heterostructure for Designing Highly Luminescent Cs–Pb–Br Perovskites. *Nat. Commun.* **2022**, *13*, 4263.
- (35) Kim, Y.-H.; Wolf, C.; Kim, Y.-T.; Cho, H.; Kwon, W.; Do, S.; Sadhanala, A.; Park, C. G.; Rhee, S.-W.; Im, S. H.; Friend, R. H.; Lee, T.-W. Highly Efficient Light-Emitting Diodes of Colloidal Metal–Halide Perovskite Nanocrystals beyond Quantum Size. *ACS Nano* **2017**, *11*, 6586–6593.
- (36) Ma, G.; Tang, S.-H.; Sun, W.; Shen, Z.; Huang, W.; Shi, J. Size-Dependent Excited State Properties of CdS Nanocrystals. *Phys. Lett. A* **2002**, *299*, 581–585.
- (37) Kim, Y. H.; Wolf, C.; Kim, H.; Lee, T.-W. Charge Carrier Recombination and Ion Migration in Metal-Halide Perovskite Nanoparticle Films for Efficient Light-Emitting Diodes. *Nano Energy* **2018**, *52*, 329–335.
- (38) Richter, J. M.; Abdi-Jalebi, M.; Sadhanala, A.; Tabachnyk, M.; Rivett, J. P. H.; Pazos-Outón, L. M.; Gödel, K. C.; Price, M.; Deschler, F.; Friend, R. H. Enhancing Photoluminescence Yields in Lead Halide Perovskites by Photon Recycling and Light Out-Coupling. *Nat. Commun.* **2016**, *7*, 13941.
- (39) Kim, Y.-H.; Cho, H.; Heo, J. H.; Im, S. H.; Lee, T.-W. Effects of Thermal Treatment on Organic-Inorganic Hybrid Perovskite Films and Luminous Efficiency of Light-Emitting Diodes. *Curr. Appl. Phys.* **2016**, *16*, 1069–1074.

□ Recommended by ACS

One-Pot Synthesis of Stable $\text{CsPbBr}_3@\text{CsPb}_2\text{Br}_5$ Core–Shell Heteronanocrystals with Controlled Permeability to Halide Ions

Ignacio Rosa-Pardo, Julia Pérez-Prieto, et al.

AUGUST 29, 2023
CHEMISTRY OF MATERIALS

READ ▶

Surfactant-Dependent Bulk Scale Mechanochemical Synthesis of CsPbBr_3 Nanocrystals for Plastic Scintillator-Based X-ray Imaging

Joydip Ghosh, Paul Sellin, et al.

AUGUST 07, 2023
ACS APPLIED NANO MATERIALS

READ ▶

Ultrastable $\text{CsPbBr}_3@\text{CsPb}_2\text{Br}_5@\text{TiO}_2$ Composites for Photocatalytic and White Light-Emitting Diodes

Chen Zhang, Arshad Saleem Bhatti, et al.

JULY 16, 2023
ACS APPLIED MATERIALS & INTERFACES

READ ▶

One-Pot Synthesis of All-Inorganic CsPbClBr_2 Blue Perovskite Quantum Dots via Stoichiometric Precursor

Jin Young Kim, Dong Hwan Wang, et al.

JULY 10, 2023
INORGANIC CHEMISTRY

READ ▶

Get More Suggestions >